Feasibility study of high-resolution coherent diffraction microscopy using synchrotron x rays focused by Kirkpatrick–Baez mirrors

Yukio Takahashi, Yoshinori Nishino, Hidekazu Mimura, Ryosuke Tsutsumi, Hideto Kubo, Tetsuya Ishikawa, and Kazuto Yamauchi

Citation: Journal of Applied Physics **105**, 083106 (2009); doi: 10.1063/1.3108997
View online: http://dx.doi.org/10.1063/1.3108997
View Table of Contents: http://scitation.aip.org/content/aip/journal/jap/105/8?ver=pdfcov
Published by the AIP Publishing

Feasibility study of high-resolution coherent diffraction microscopy using synchrotron x rays focused by Kirkpatrick–Baez mirrors

Yukio Takahashi,[1,a)] Yoshinori Nishino,[2] Hidekazu Mimura,[3] Ryosuke Tsutsumi,[3] Hideto Kubo,[3] Tetsuya Ishikawa,[2] and Kazuto Yamauchi[3,4]
[1]*Frontier Research Base for Global Young Researchers, Frontier Research Center, Graduate School of Engineering, Osaka University, 2-1 Yamada-oka, Suita, Osaka 565-0871, Japan*
[2]*RIKEN SPring-8 Center, Kouto, Sayo, Sayo, Hyogo 679-5148, Japan*
[3]*Department of Precision Science and Technology, Graduate School of Engineering, Osaka University, 2-1 Yamada-oka, Suita, Osaka 565-0871, Japan*
[4]*Research Center for Ultra-Precision Science and Technology, Graduate School of Engineering, Osaka University, 2-1 Yamada-oka, Suita, Osaka 565-0871, Japan*

(Received 6 January 2009; accepted 23 February 2009; published online 23 April 2009)

High-flux coherent x rays are necessary for the improvement of the spatial resolution in coherent x-ray diffraction microscopy (CXDM). In this study, high-resolution CXDM using Kirkpatrick–Baez (KB) mirrors is proposed, and the mirrors are designed for experiments of the transmission scheme at SPring-8. Both the photon density and spatial coherence of synchrotron x rays focused by the KB mirrors are investigated by wave optical simulation. The KB mirrors can produce nearly diffraction-limited two-dimensional focusing x rays of ~ 1 μm in size at 8 keV. When the sample size is less than ~ 1 μm, the sample can be illuminated with full coherent x rays by adjusting the cross-slit size set between the source and the mirrors. From the estimated photon density at the sample position, the feasibility of CXDM with a sub-1-nm spatial resolution is suggested. The present ultraprecise figuring process enables us to fabricate mirrors for carrying out high-resolution CXDM experiments. © *2009 American Institute of Physics*. [DOI: 10.1063/1.3108997]

I. INTRODUCTION

Coherent x-ray diffraction microscopy[1,2] (CXDM) is a lensless x-ray imaging technique using coherent x-ray scattering. The sample is illuminated with coherent x rays, and its far-field diffraction pattern is recorded. The wave field behind the sample is reconstructed by applying a phase retrieval algorithm, e.g., Fienup's hybrid input-output algorithm,[3] to the diffraction pattern. CXDM was experimentally demonstrated by Miao *et al.*[1] in 1999 and, since then, various CXDM studies have been performed using synchrotron radiation,[4–11] tabletop high-harmonic soft x rays,[12] and a vacuum ultraviolet free-electron laser.[13–15] In principle, CXDM can provide us images with a spatial resolution down to one-half the wavelength of the incident x ray. To reconstruct high-resolution images, high-Q diffraction data must be experimentally obtained[16] or mathematically estimated from the measured low-Q data,[17] where Q is the magnitude of the scattering vector. Since the diffraction intensity decays with the power law $Q^{-\alpha}$ ($\alpha \approx 4$), the sample must be illuminated with high-flux coherent x rays to collect high-Q diffraction data. The high-flux coherent x rays are important not only for the improvement of the spatial resolution but also for quick measurements. The quick measurements enable us to trace a fast process in dynamical samples. An effective method for obtaining the high-flux coherent x rays is to highly focus x rays using optical devices. In 2006, Quiney *et al.* proposed the use of highly focused x-ray fields in CXDM and imaged the complex field at the focus of a Fresnel zone plate (FZP).[18] Until now, Fresnel coherent diffractive imaging,[7] keyhole coherent diffractive imaging,[10] and ptychographic imaging[11] have been performed in CXDM experiments using FZP. Very recently, by using focusing x rays with a refractive lens, a CXDM experiment has achieved a resolution of about 5 nm in 600 s exposure time.[19] The importance of focusing devices in CXDM has been increasing. In this study, we propose high-resolution CXDM using synchrotron x rays focused by total reflection mirrors.

Kirkpatrick–Baez (KB) mirrors,[20] which consist of two elliptical mirrors, are a promising x-ray focusing device. Recently, x rays of 15 keV have been two-dimensionally focused to a 36×48 nm^2 spot[21] by KB mirrors and one-dimensionally focused to a 25-nm-wide line[22] by an elliptical mirror. A scanning x-ray fluorescence microscope equipped with KB mirrors has been developed[23] and used for biological imaging.[24] X-ray free-electron lasers (XFELs), which are next-generation x-ray sources, are constructed at several facilities around the world. XFELs are predicted to provide extremely intense femtosecond-pulse x rays with an almost full spatial coherence that is convenient for high-resolution and/or time-resolved CXDM experiments. Total reflection mirrors are considered to be the best focusing optics for XFELs because of their high efficiency and radiation hardness. Recently, x rays of 15 keV have been one-dimensionally focused to a 75-nm-wide line by a 400-mm-long elliptical mirror that was developed for use in XFEL facilities.[25] The use of KB mirrors in CXDM was first reported in an experiment using Bragg reflection in a synchrotron facility.[26] In this study, KB mirrors are designed for typical CXDM experiments of the transmission scheme at

[a)]Author to whom correspondence should be addressed. Electronic mail: takahashi@wakate.frc.eng.osaka-u.ac.jp.

TABLE I. Parameters of designed elliptical mirrors.

	First mirror	Second mirror
Maximum glancing angle (mrad)	1.30	1.05
Acceptance width (μm)	113	90
Focal length (mm)	600	495
Length of major axis (m)	48.600	48.600
Length of minor axis (mm)	6.708	4.880

BL29XUL in SPring-8. The properties of the synchrotron x rays focused by the mirrors are investigated by wave optical simulation. The feasibility of high-resolution CXDM using KB focusing x rays is discussed.

II. DESIGN OF ELLIPTICAL MIRRORS

In CXDM experiments, a sample must be illuminated with x rays with a well-defined wavefront, such as a plane wave. The diffraction-limited focusing x rays produced by an ultraprecisely figured mirror can almost be regarded as a plane wave.[27] If the sample size is less than the focused beam size, ideal coherent x-ray diffraction measurements are realized in principle. The typical sample size and x-ray energy range in previous CXDM experiments of the transmission scheme are ~1 μm and 5–15 keV, respectively. Therefore, KB mirrors were designed to produce diffraction-limited focused x rays of ~1 μm size at an incident x-ray energy of 8 keV. In addition, to obtain a high photon density at the focus, a large geometrical demagnification of the source was considered. Table I shows a summary of the parameters of the elliptical mirrors designed for the CXDM experiments at BL29XUL (Ref. 28) in SPring-8. The material of the mirrors is fused silica. The maximum glancing angles of the first and second mirrors are 1.30 and 1.05 mrad, respectively. More than 99% of the x rays at 8 keV reflect on the mirror surface when the surface is ideal. The mirror length and width are 90 and 4 mm, respectively. The synchrotron x rays are vertically focused by the first mirror and horizontally focused by the second mirror.

III. SIMULATIONS

The properties of synchrotron x rays focused by the designed mirrors were evaluated by numerical simulation. Synchrotron x rays are regarded as partially coherent x rays emitted by a chaos light source. The partial coherence is separately treated by considering the temporal and spatial coherence concepts. In the present simulation, completely monochromatic x rays of 8 keV, i.e., the temporal coherence length is infinitely large, were considered. The spatial coherence was considered by calculating the propagation of x rays from a finite source. Figure 1 shows the schematic view of the source, mirror, and slit arrangement for the present simulation that considers the experiment at BL29XUL in SPring-8. The size of the light source in the synchrotron radiation is given by that of the electron beam. The size, which is defined as the width of the Gaussian distribution, is determined to be 301 μm in the vertical direction and 6 μm in the horizontal direction when all of the gaps of insertion devices are opened.[29] The above value was used as the size of the light source in the simulation. The propagation of x-ray spherical waves emitted by each point of the source was calculated. The mirror reflectivity was assumed to be 100%. At observation points, the sum of the intensity distributions of the x rays propagating from all points of the source was calculated. A cross slit was additionally set 52 m downstream of the source to control the x-ray coherence length downstream of the slit. The cross-slit size was defined as C_x and C_z in the horizontal and vertical directions, respectively. Previous CXDM measurements, using x rays going through a pinhole, have been carried out at a space just after the slit, i.e., experimental hutch 1 (EH1) at BL29XUL. The present simulation assumes that coherent x-ray diffraction measurements using KB mirrors are carried out in experimental hutch 2 (EH2) at BL29XUL. The first mirror was set 48 m downstream of the cross slit in EH2. The focal profiles in the horizontal and vertical directions were calculated. To evaluate the spatial coherence of x rays in the focal plane, interference fringes from Young's double slit were calculated. The interval of the double slit and the amount of displacement from the optical axis were defined as Y and ΔY, respectively. Fringe visibility, defined as $(I_{\max}-I_{\min})/(I_{\max}+I_{\min})$, was derived from the interference pattern, where $I_{\max}$ and $I_{\min}$ are the maximum and minimum intensities of the interference pattern, respectively.

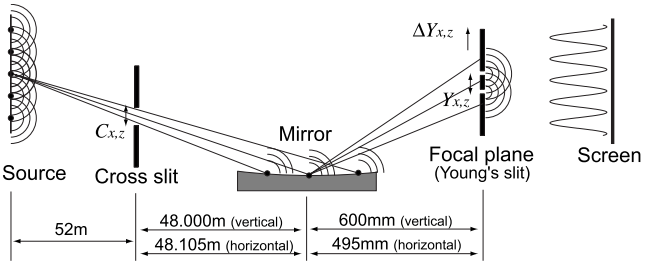

FIG. 1. Schematic view of source, elliptical mirror, and slit arrangement in the present simulation. x and z correspond to the horizontal and vertical directions, respectively.

A. Focal profile and photon density

Figures 2(a) and 2(b) show the density profiles of the x rays focused by the first and second mirrors with ideal surfaces, respectively. The photon density was normalized by the averaged density of x-ray photons immediately after passing through the cross slit. The photon density at the focal point in the horizontal direction is on the order of magnitude smaller than that in the vertical direction, owing to the difference in the spatial coherence of x rays between both directions. Figures 2(c) and 2(d) show the C dependences of both the peak-top value and full width at half maximum (FWHM) of the profile in the vertical and horizontal directions, respectively. The FWHM increases with increasing C, which is a typical feature of focusing x rays observed also in previous experiments,[23] and approaches a constant value with decreasing C. This implies that the focused beam approaches the diffraction limit as the slit size decreases. In the

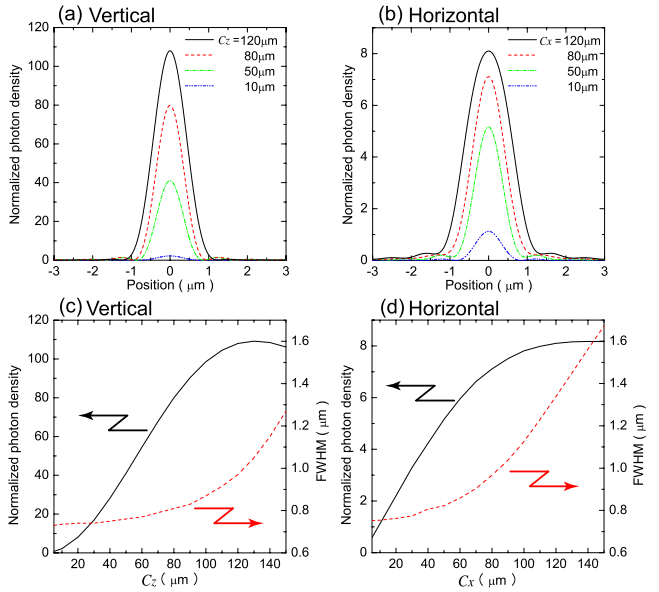

FIG. 2. (Color online) [(a) and (b)] Photon density profiles of x rays focused by (a) first and (b) second mirrors in Table I, which are calculated one dimensionally in the vertical and horizontal directions when cross-slit sizes (C) are 10, 50, 80, and 120 μm in arrangement drawn in Fig. 1. The photon density is normalized by the averaged photon density of x rays immediately after passing through the cross slit. [(c) and (d)] C dependences of both peak-top value and FWHM of profiles in the (c) vertical and (d) horizontal directions.

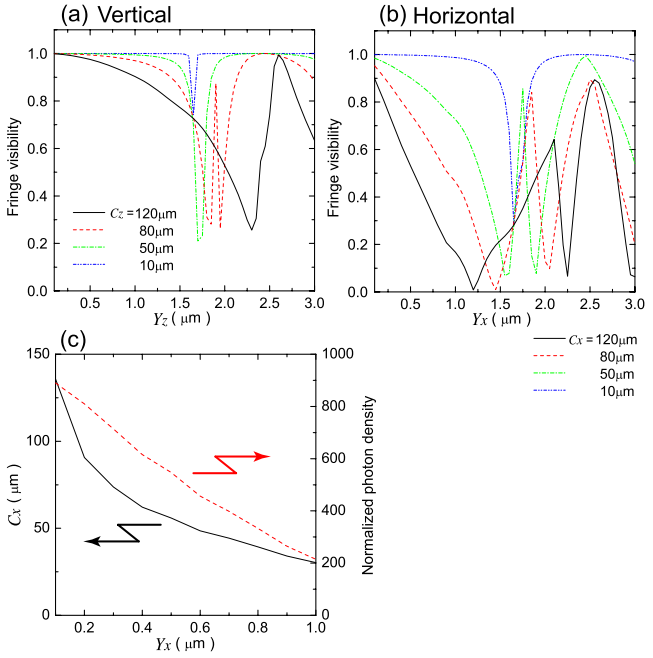

FIG. 3. (Color online) [(a) and (b)] Double-slit interval (Y) dependences of visibility calculated in the (a) vertical and (b) horizontal directions. The center of the double slit is on the optical axis. (c) Relationship between Y_x and C_x when visibility becomes 0.88, and photon density of two-dimensionally focusing x rays at each C_x. C_z is fixed at 131 μm.

vertical direction, the photon density decreases when C_z is more than 131 μm, owing to the reduction in focusing efficiency.

B. Spatial coherence

Figures 3(a) and 3(b) show the Y dependences of the fringe visibility in the vertical and horizontal directions, respectively. Here, the mirror surface is assumed to be ideal. In both directions, when C is 10 μm, a visibility of more than 0.88, which is sometimes regarded as coherent illumination, is obtained within the main peak. The visibility decreases rapidly at $Y=1.65$ μm, which is almost consistent with the interval between the first minimum points of the focal profile. This is because the phase difference for the first minimum points markedly changes, depending on the emitting points in the source. As C increases, i.e., the spatial coherence length decreases, the area of the visibility of more than 0.88 within the main peak decreases and the variation in visibility at $Y \geqslant 1.5$ μm becomes complex. The visibility in the horizontal direction markedly decreases compared to that in the vertical direction. To illuminate samples with fully coherent x rays, the sample size must be less than ~1 μm. The cross-slit size must be adjusted in accordance with the sample size.

Figure 3(c) shows the relationship between Y_x and C_x when the visibility becomes 0.88, and the photon density of two-dimensionally focusing x rays at each C_x. The normalized photon density was averaged within each double-slit interval. C_z is fixed at 131 μm to obtain the visibility of more than 0.88 in the vertical direction when Y_z is less than 1 μm. When Y_x is 100 nm, coherent x rays with a photon density ~900 times larger than that of x rays immediately after passing through the cross slit can be produced. In the previous CXDM measurement, a pinhole of 20 μm diameter is set immediately after the cross slit. The sample is positioned ~1 m downstream of the pinhole. The photon density of x rays at the sample position decreases by ~15% compared to that of x rays immediately after passing through the cross slit, which was estimated by simulation. Therefore, if the sample size is 100 nm, the sample can be illuminated with coherent x rays with a photon density ~1000 times larger than that in a previous CXDM measurement. By considering that a 7 nm resolution in 50 min exposure time is achieved in the previous measurement at EH1 of BL29XUL in SPring-8,[16] it can be considered that a sub-1-nm resolution for an exposure time of more than 120($\approx 7^4/1000\times 50$) min is realized.

The distribution of the spatial coherence in the focal plane was also examined. Figure 4 shows the ΔY dependences of the visibility at Y values of 0.1 and 1.0 μm. When $Y=1.0$ μm in both directions, the area of the visibility of more than 0.88 is smaller than that obtained when $Y=0.1$ μm. As the center of the double slit separates from the focus, the visibility once decreases and increases again. From these plots, the accuracy required for the sample alignment can be estimated. When the sample size is 0.1 μm, the sample must be aligned within less than ~0.5 μm from the focus. When the sample size is 1.0 μm, the sample must be aligned within less than ~50 nm from the focus. Therefore, when the sample size is close to the width of the focal profile, both the accurate alignment and high stability of the position are required.

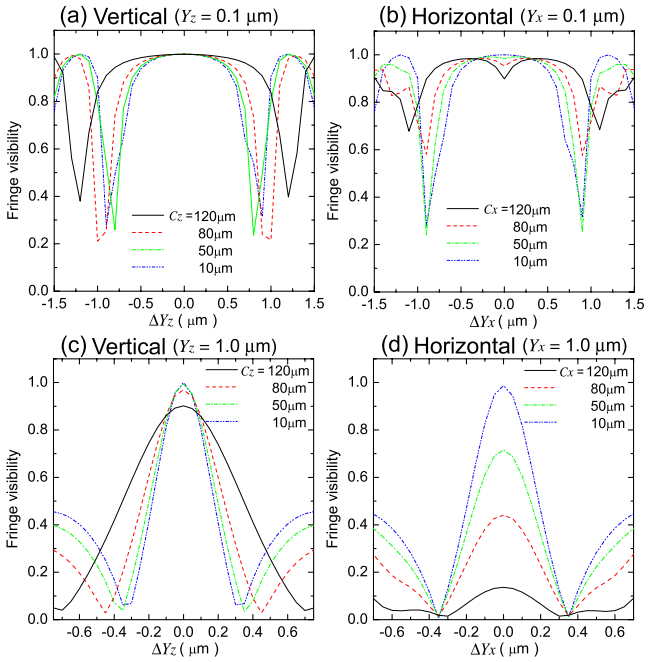

FIG. 4. (Color online) Double-slit shift (ΔY) dependences of visibility in the vertical and horizontal directions when double-slit intervals are 0.1 and 1.0 μm.

C. Effects of figure errors of mirror

The effects of figure errors of the designed mirror on both the focal profile and spatial coherence were examined. Figure 5(a) shows the figure error profiles characterized in short and long spatial wavelength ranges in the longitudinal direction of the first mirror. When the peak-to-valley (PV) figure error heights were 5.0, 10.0, 20.0, and 40.0 nm, both the photon density profile and fringe visibility of x rays focused by the first mirror were calculated. The root mean square (rms) figure errors are 1.5, 3.0, 6.0, and 12.0 nm for the surfaces with PV figure error heights of 5.0, 10.0, 20.0, and 40.0 nm error, respectively. It is well known that the mirror reflectivity decreases owing to the rms figure error. Under the present condition, i.e., the glancing angle is less than 1.3 mrad and the incident x-ray energy is 8 keV, the decrease in reflectivity due to the rms figure errors is less than 5.0%.[30]

Figures 5(b) and 5(c) show the density profiles of the x rays focused by the first mirror with figure errors in short and long spatial wavelength ranges, respectively. C_z was fixed at 120 μm. According to Rayleigh's quarter wavelength rule,[31] if the wavefront aberration error of an optical device is less than $1/4\lambda$, where λ is the wavelength, the focal profile does not change markedly. In the present case, $1/4\lambda$ for the PV phase error height corresponds to a PV figure error of ~15 nm. The density profile of x rays focused by the mirror with a 5 nm PV figure error is nearly equal to that of x rays focused by the ideal mirror. As the PV figure error increases, the photon density within the main peak decreases. The figure error in the short spatial wavelength range causes the increase in the photon density of higher order satellite peaks, while that in the long spatial wavelength range causes both the peak shifts and the increase in the photon density near the main peak.

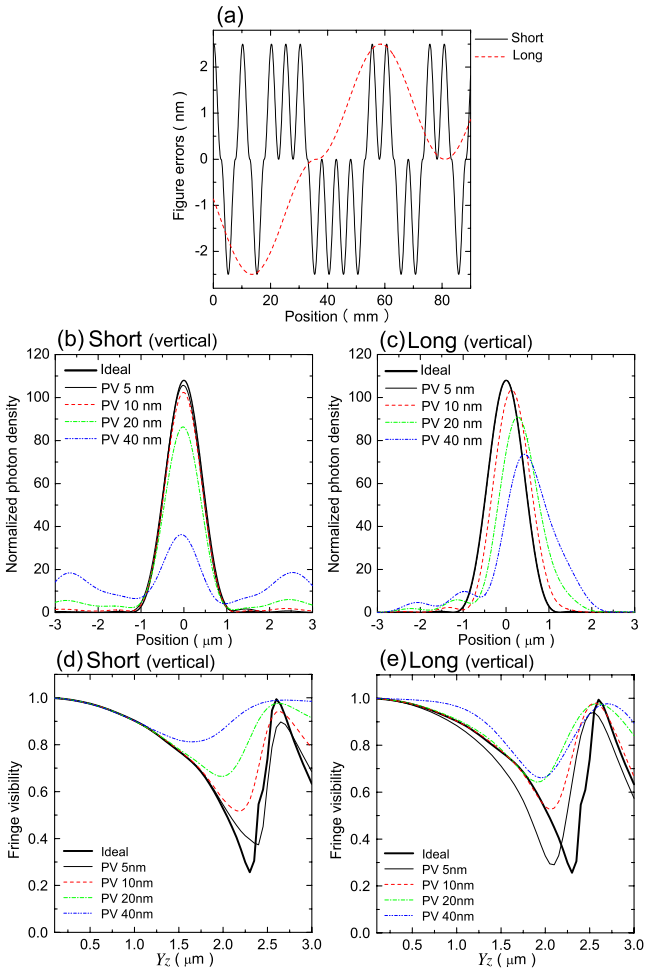

FIG. 5. (Color online) (a) Figure error profiles characterized in short and long spatial wavelength ranges. The PV figure error height is 5 nm. [(b) and (c)] Photon density profiles of x rays focused by first mirror with PV figure errors of 5.0, 10.0, 20.0, and 40.0 nm in short and long spatial wavelength ranges. [(d) and (e)] Double-slit interval (Y) dependences of fringe visibility for focused x rays of (b) and (c). The center of the double slit is aligned to make it equal to the center of each main peak.

Figures 5(d) and 5(e) show the Y_z dependences of the fringe visibility for the focused x rays shown in Figs. 5(b) and 5(c), respectively. Even if the photon density at the focus becomes below half or the focal position shifts owing to the figure errors, the fringe visibility hardly changes within the main peak. It is understood that the spatial coherence is ensured within the main peak even if the focal profile is not ideal. Now, the fabrication of x-ray mirrors with PV figure errors less than 1 nm and rms figure errors less than 0.5 nm is realized by ultraprecise figuring processes, such as elastic emission machining[32–34] (EEM). Thus, by using the mirrors fabricated by EEM, CXDM experiments can be performed.

IV. CONCLUSION

We proposed the use of KB mirrors in CXDM experiments of the transmission scheme and designed the KB mirrors for the experiments at BL29XUL in SPring-8. As a result of wave optical simulation, the designed KB mirrors can produce nearly diffraction-limited two-dimensional focused x rays of ~1 μm size at 8 keV. The spatial coherence of the focusing x rays can be controlled by adjusting the size of the

cross slit set between the source and the first mirror. When the sample size is less than 100 nm, the photon density of the x rays irradiated to the sample becomes ~1000 times larger than that in previous experiments at BL29XUL, and hence, CXDM with a sub-1-nm spatial resolution can possibly be realized. By using the mirrors fabricated by the present ultraprecise figuring process, CXDM experiments using synchrotron x rays focused by KB mirrors can be conducted.

In this paper, the feasibility of using KB mirrors to focus coherent x rays to a spot size of ~1 μm was investigated. However, there are also interesting samples more than 1 μm such as biological cells and cellular organelles. Even if the spot size is ~1 μm, images of bigger samples than 1 μm can be reconstructed by using the ptychographic method.[11] In CXDM studies using XFEL, it is estimated that a sample is broken by illumination of a single pulse x ray. In this case, some KB mirrors to focus coherent x rays to different spot size should be prepared. According to the sample size, it is necessary to use the optimal setup. We believe that high-resolution CXDM using KB focusing x rays can open up new frontiers of structural studies with an x-ray microscope.

ACKNOWLEDGMENTS

This research has been carried out at the Frontier Research Base for Global Young Researchers, Osaka University, on the Program of Promotion of Environmental Improvement to Enhance Young Researcher's Independence, the Special Coordination Funds for Promoting Science and Technology, from the Ministry of Education, Culture, Sports, Science and Technology (MEXT). This work was also partly supported by funds from a Grant-in-Aid for the "Promotion of X-ray Free Electron Laser Research," Specially Promoted Research (Grant No. 18002009), the Global COE Program "Center of Excellence for Atomically Controlled Fabrication Technology" from MEXT, Konica Minolta Imaging Science Foundation, and Shimadzu Science Foundation. The authors would like to acknowledge S. Matsuyama, S, Handa, and T. Kimura for valuable discussions.

[1]J. Miao, P. Charalambous, J. Kirz, and D. Sayre, Nature (London) **400**, 342 (1999).
[2]M. A. Pfeifer, G. J. Williams, I. A. Vartanyants, R. Harder, and I. K. Robinson, Nature (London) **442**, 63 (2006).
[3]J. R. Fienup, Appl. Opt. **21**, 2758 (1982).
[4]J. Miao, K. O. Hodgson, T. Ishikawa, C. A. Larabell, M. A. LeGros, and Y. Nishino, Proc. Natl. Acad. Sci. U.S.A. **100**, 110 (2003).
[5]D. Shapiro, P. Thibault, T. Beetz, V. Elser, M. Howells, C. Jacobsen, J. Kirz, E. Lima, H. Miao, A. M. Neiman, and D. Sayre, Proc. Natl. Acad. Sci. U.S.A. **102**, 15343 (2005).
[6]J. Miao, C.-C. Chen, C. Song, Y. Nishino, Y. Kohmura, T. Ishikawa, D. Ramunno-Johnson, T.-K. Lee, and S. H. Risbud, Phys. Rev. Lett. **97**, 215503 (2006).
[7]G. J. Williams, H. M. Quiney, B. B. Dhal, C. Q. Tran, K. A. Nugent, A. G. Peele, D. Paterson, and M. D. de Jonge, Phys. Rev. Lett. **97**, 025506 (2006).
[8]Y. Takahashi, Y. Nishino, T. Ishikawa, and E. Matsubara, Appl. Phys. Lett. **90**, 184105 (2007).
[9]J. M. Rodenburg, A. C. Hurst, A. G. Cullis, B. R. Dobson, F. Pfeiffer, O. Bunk, C. David, K. Jefimovs, and I. Johnson, Phys. Rev. Lett. **98**, 034801 (2007).
[10]B. Abbey, K. A. Nugent, G. J. Williams, J. N. Clark, A. G. Peele, M. A. Pfeifer, M. de Jonge, and I. McNulty, Nat. Phys. **4**, 394 (2008).
[11]P. Thibault, M. Dierolf, A. Menzel, O. Bunk, C. David, and F. Pfeiffer, Science **321**, 379 (2008).
[12]R. L. Sandberg, A. Paul, D. A. Raymondson, S. Hädrich, D. M. Gaudiosi, J. Holtsnider, R. I. Tobey, O. Cohen, M. M. Murnane, H. C. Kapteyn, C. Song, J. Miao, Y. Liu, and F. Salmassi, Phys. Rev. Lett. **99**, 098103 (2007).
[13]H. N. Chapman, A. Barty, M. J. Bogan, S. Boutet, M. Frank, S. P. Hau-Riege, S. Marchesini, B. W. Woods, S. Bajt, W. H. Benner, R. A. London, E. Plönjes, M. Kuhlmann, R. Treusch, S. Düsterer, T. Tschentscher, J. R. Schneider, E. Spiller, T. Möller, C. Bostedt, M. Hoener, D. A. Shapiro, K. O. Hodgson, D. V. D. Spoel, F. Burmeister, M. Bergh, C. Chaleman, G. Huldt, M. M. Seibert, F. R. N. C. Maia, R. W. Lee, A. Szöke, N. Timneanu, and J. Hajdu, Nat. Phys. **2**, 839 (2006).
[14]M. J. Bogan, W. H. Benner, S. Boutet, U. Rohner, M. Frank, A. Barty, M. M. Seibert, F. Maia, S. Marchesini, S. Bajt, B. Woods, V. Riot, S. P. Hau-Riege, M. Svenda, E. Marklund, E. Spiller, J. Hajdu, and H. N. Chapman, Nano Lett. **8**, 310 (2008).
[15]A. Barty, S. Boutet, M. J. Bogan, S. Hau-Riege, S. Marchesini, K. Sokolowski-Tinten, N. Stojanovic, R. Tobey, H. Ehrke, A. Cavalleri, S. Düsterer, M. Frank, S. Bajt, B. W. Woods, M. M. Seibert, J. Hajdu, R. Treusch, and H. N. Chapman, Nat. Photonics **1**, 336 (2008).
[16]J. Miao, T. Ishikawa, E. H. Anderson, and K. O. Hodgson, Phys. Rev. B **67**, 174104 (2003).
[17]Y. Takahashi, Y. Nishino, and T. Ishikawa, Phys. Rev. A **76**, 033822 (2007).
[18]H. M. Quiney, A. G. Peele, Z. Cai, D. Paterson, and K. A. Nugent, Nat. Phys. **2**, 101 (2006).
[19]C. G. Schroer, P. Boye, J. M. Feldkamp, J. Patommel, A. Schropp, A. Schwab, S. Stephan, M. Burghammer, S. Schoder, and C. Riekel, Phys. Rev. Lett. **101**, 090801 (2008).
[20]P. Kirkpatrick and A. V. Baez, J. Opt. Soc. Am. **38**, 766 (1948).
[21]H. Mimura, S. Matsuyama, H. Yumoto, H. Hara, K. Yamamura, Y. Sano, M. Shibahara, K. Endo, Y. Mori, Y. Nishino, K. Tamasaku, M. Yabashi, T. Ishikawa, and K. Yamauchi, Jpn. J. Appl. Phys., Part 1 **44**, 539 (2005).
[22]H. Mimura, H. Yumoto, S. Matsuyama, Y. Sano, K. Yamamura, Y. Mori, M. Yabashi, Y. Nishino, K. Tamasaku, T. Ishikawa, and K. Yamauchi, Appl. Phys. Lett. **90**, 051903 (2007).
[23]S. Matsuyama, H. Mimura, H. Yumoto, Y. Sano, K. Yamamura, M. Yabashi, Y. Nishino, K. Tamasaku, T. Ishikawa, and K. Yamauchi, Rev. Sci. Instrum. **77**, 103102 (2006).
[24]M. Shimura, A. Saito, S. Matsuyama, T. Sakuma, Y. Terui, K. Ueno, H. Yumoto, K. Yamauchi, K. Yamamura, H. Mimura, Y. Sano, M. Yabashi, K. Tamasaku, K. Nishio, Y. Nishino, K. Endo, K. Hatake, Y. Mori, Y. Ishizaka, and T. Ishikawa, Cancer Res. **65**, 4998 (2005).
[25]H. Mimura, S. Morita, T. Kimura, D. Yamakawa, W. Lin, Y. Uehara, S. Matsuyama, H. Yumoto, H. Ohashi, K. Tamasaku, Y. Nishino, M. Yabashi, T. Ishikawa, H. Ohmori, and K. Yamauchi, Rev. Sci. Instrum. **79**, 083104 (2008).
[26]L.-M. Stadler, R. Harder, I. K. Robinson, C. Rentenberger, H. P. Karnthaler, B. Sepiol, and G. Vogl, Phys. Rev. B **76**, 014204 (2007).
[27]H. Mimura, H. Yumoto, S. Matsuyama, S. Handa, T. Kimura, Y. Sano, M. Yabashi, Y. Nishino, K. Tamasaku, T. Ishikawa, and K. Yamauchi, Phys. Rev. A **77**, 015812 (2008).
[28]K. Tamasaku, Y. Tanaka, M. Yabashi, H. Yamazaki, N. Kawamura, M. Suzuki, and T. Ishikawa, Nucl. Instrum. Methods Phys. Res. A **467-468**, 686 (2001); see also BL29XUL outline in SPring-8 website http://www.spring8.or.jp.
[29]See accelerator overview in SPring-8 website http://www.spring8.or.jp.
[30]B. L. Henke, E. M. Gullikson, and J. C. Davis, At. Data Nucl. Data Tables **54**, 181 (1993).
[31]M. Born and E. Wolf, *Principle of Optics*, 7th ed. (Cambridge University Press, Cambridge, 2001).
[32]Y. Mori, K. Yamauchi, and K. Endo, Precis. Eng. **9**, 123 (1987).
[33]Y. Mori, K. Yamauchi, and K. Endo, Precis. Eng. **10**, 24 (1988).
[34]K. Yamauchi, H. Mimura, K. Inagaki, and Y. Mori, Rev. Sci. Instrum. **73**, 111 (2002).